Volume 17
Number 14
15 April 2026
Pages 6789–7324

Chemical Science

rsc.li/chemical-science

ISSN 2041-6539

ROYAL SOCIETY OF CHEMISTRY

EDGE ARTICLE

Alexandru Vlad *et al.*

Decoupling ion size from electrochemistry: cation-size-independent accommodation of Li^+ to Cs^+ in an amorphous sulfonamide coordination polymer

Chemical Science

ROYAL SOCIETY OF CHEMISTRY

EDGE ARTICLE

View Article Online
View Journal | View Issue

Cite this: *Chem. Sci.*, 2026, **17**, 6924

All publication charges for this article have been paid for by the Royal Society of Chemistry

Decoupling ion size from electrochemistry: cation-size-independent accommodation of Li^+ to Cs^+ in an amorphous sulfonamide coordination polymer

Robert Markowski,[a] Darsi Rambabu,[a] Augustin Ramackers[a] and Alexandru Vlad *[ab]

Received 21st January 2026
Accepted 9th March 2026

DOI: 10.1039/d6sc00585c

rsc.li/chemical-science

Understanding how cation identity governs charge storage is critical for next-generation batteries beyond lithium. Here we show that the amorphous Ca–Zn–PTtSA coordination polymer functions as a universal host for reversible electrochemical storage of all alkali-metal cations from Li^+ to Cs^+, including the rare case of reversible Rb^+ and Cs^+ electrochemical cycling in a positive electrode material. Despite the large variation in ionic radius, all cations yield nearly identical redox potentials, full material utilization (~95 mAh g^{-1}), and low hysteresis. Elemental and spectroscopic analyses confirm a cation storage mechanism without solvent co-intercalation. This behavior originates from the framework's amorphous flexibility and the delocalized electronic structure of the conjugated sulfonamide ligand, which together enable weak, reversible metal–ligand interactions and fast cation transport ($D \approx 10^{-9}$ cm^2 s^{-1}). Consequently, M_2–Zn–PTtSA delivers high-rate capability and long-term cycling stability across the entire alkali-metal series, providing a platform that decouples ion size from electrochemical performance and supports "cation-of-choice" battery chemistries.

Introduction

Organic electrode materials emerge as attractive candidates for next-generation energy storage, owing to their structural tunability, sustainability, and ability to support multi-electron redox chemistry.[1–6] A key challenge, however, is the scarcity of versatile hosts capable of accommodating a wide range of cations.[7,8] This constraint arises from the different ionic sizes of charge carriers. For example, moving from Li^+ to Na^+ or Ca^{2+} systems requires different degrees of structural flexibility in the host material imposed by the coordination environment of hosted cations.[9,10] While crystalline materials often impose size and structural restrictions, low-crystallinity or amorphous phases can more readily adapt to larger ions.[11–13] For instance, crystalline Zn-DOBDP (Zn-(2,5-dioxido-1,4-benzenediphosphonate) can store Li^+ and Na^+, but not K^+, underscoring the importance of lattice adaptability.[14] Amorphous materials, both inorganic and organic compositions, have therefore attracted growing attention as electrode hosts. Their intrinsically disordered network enhances cation mobility and enables reversible storage of large ions.[15–17] A representative example is amorphous iron phosphate, which can host Li^+, Na^+, K^+, Zn^{2+}, and Mg^{2+}, whereas its crystalline analog shows limited capability for Na^+ storage.[12] Nevertheless, gradual crystallization during cycling has been found to undermine the long-term stability.

Among organic electrodes, only a few systems have demonstrated broad cation compatibility. For instance, polyimides and polyanthraquinones have been shown to reversibly accommodate Li^+, Na^+, K^+, Mg^{2+}, and Ca^{2+}.[18–21] However, as the cation size increases, these materials typically exhibit reduced utilization and rapid capacity fading, even under moderate cycling rates. In addition, most are used primarily from their oxidized phases (cation free), and reports of amorphous cation-reservoir organic materials remain scarce. Finally, many of these electrodes primarily host solvated or ion-paired cations, which can reduce their practical energy densities.

To address this gap, we recently introduced conjugated sulfonamide (CSA) coordination polymers derived from benzene-1,2,4,5-tetrayltetrakis(methylsulfonylamide) (H_4–PTtSA), a Wurster-type redox center.[6] These materials have demonstrated the ability to host not only monovalent cations but also divalent cations.[7,8,15] To date, only two amorphous organic systems with such multi-cation storage versatility have been reported: the CSA-based materials and frameworks derived from 2,2′,5,5′-tetrahydroxy-4,4′-biphenyl dicarboxylic acid (H_6-THBPD), the latter one found to suffer nevertheless from solubility issues.[22] Notably, the amorphous sulfonamide coordination polymers uniquely combine this broad cation diversity with excellent cycling stability, fast kinetics, pure solid-

[a]*Institute of Condensed Matter and Nanosciences, Molecular Chemistry, Materials and Catalysis, Université Catholique de Louvain, Louvain-la-Neuve B-1348, Belgium. E-mail: alexandru.vlad@uclouvain.be*

[b]*WEL Research Institute, Avenue Pasteur, 6, 1300 Wavre, Belgium*

state storage, and high operating voltages, establishing them as a promising platform for multi-ion energy storage.[15]

Building on these insights, this study systematically explores the storage of 1s-block cations (M^+), from Li^+ to Cs^+, departing from an amorphous Ca–Zn–PTtSA coordination polymer phase. We show that the Ca^{2+} ions can be efficiently and quantitatively replaced *in situ* by the corresponding M^+ cations through electrochemical exchange, as confirmed by elemental analysis. We investigate how the nature of the stored cation influences key electrochemical properties, including material utilization, galvanostatic charge–discharge profiles, working potential, rate performance, and cation diffusion. The sulfonamide polymer phase is found not only to efficiently accommodate large cations such as Cs^+, which is roughly twice the size of Li^+, but also exhibit fast cation diffusion ($\sim 10^{-9}$ cm^2 s^{-1}). This high ion mobility is attributed to the weak interactions between the cations and the polymer backbone, highlighting the unique combination of broad cation compatibility and fast transport enabled by the amorphous framework.

Results and discussion

Storage mechanism

To investigate how the nature of the accommodated monovalent cation (M^+) affects electrochemical performance, we selected the Ca–Zn–PTtSA coordination polymer (Fig. 1A) as the starting electrode material, synthesized following our previously reported procedure.[15] This amorphous coordination polymer has demonstrated excellent performance in Ca^{2+} (and other divalent cations) storage, with the mechanism thoroughly studied. The coordination polymer is made of a backbone formed by the coordination of the $PTtSA^{4-}$ ligand with Zn^{2+} cations. To maintain charge balance, counter cations (in this case Ca^{2+}) are weakly coordinated to the oxygen atoms of the sulfonamide groups, giving rise to the Ca–Zn–PTtSA unit block. Using the Ca^{2+}-containing phase as the starting point allows systematic replacement of Ca^{2+} with 1s-block monovalent cations through *in situ* electrochemical cation exchange (Fig. 1B and C), enabling a direct study of how cation nature affects storage properties. This approach eliminates artifacts that could arise from differences in polymer synthesis, such as variations in solubility, structure, or topology, which would make comparisons between independently synthesized M^+ materials unreliable.

The storage mechanism of Ca–Zn–PTtSA relies on the reversible two-electron redox process of the $PTtSA^{4-}$ organic linker. During the first charge step, the $PTtSA^{4-}$ unit is oxidized to $PTtSA^{2-}$, along with the extraction of Ca^{2+}, leading to the formation of the Ca-depleted □-Zn–PTtSA phase (□ – void). If the galvanostatic cycling is performed in an electrochemical cell containing the corresponding M^+ electrolyte (*e.g.*, 1 mol L^{-1} MTFSI in propylene carbonate, PC), Ca^{2+} is removed from the framework during the first charge step, while M^+ (Li^+, Na^+, K^+,

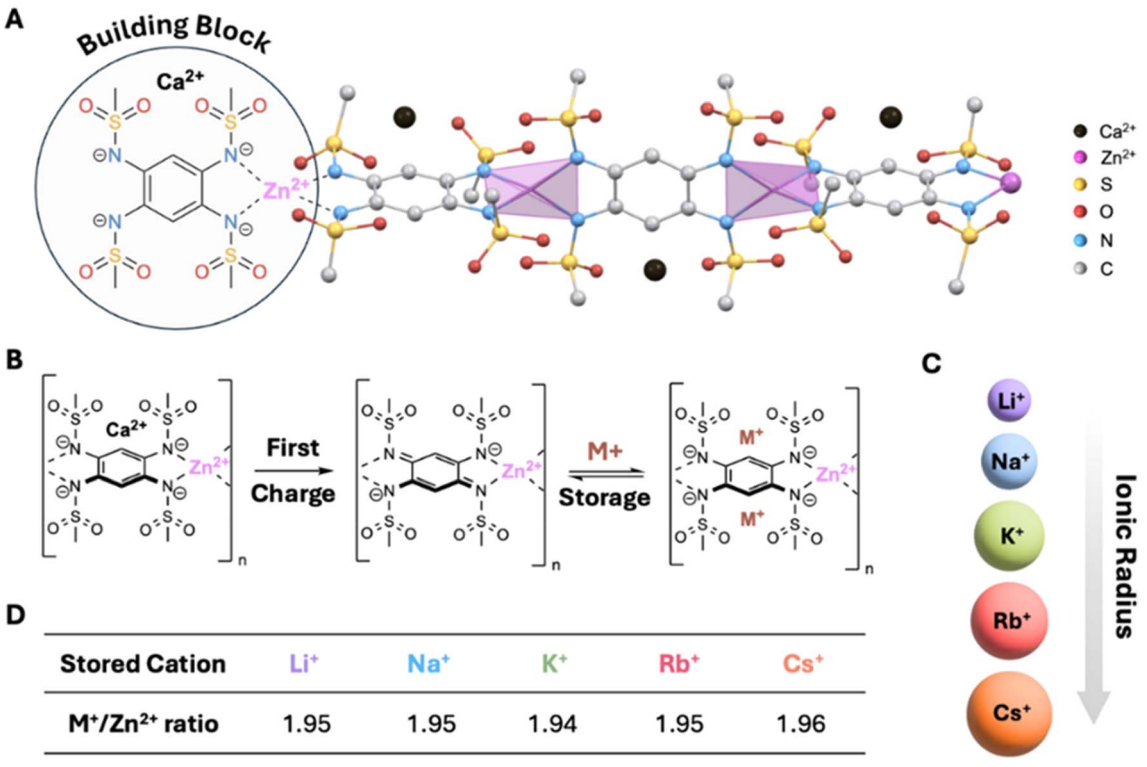

D

Stored Cation	Li^+	Na^+	K^+	Rb^+	Cs^+
M^+/Zn^{2+} ratio	1.95	1.95	1.94	1.95	1.96

Fig. 1 (A) Schematic representation of the Ca–Zn–PTtSA sulfonamide coordination polymer structure. (B) Mechanism of monovalent cation (M^+) electrochemical exchange in Ca–Zn–PTtSA. (C) Comparison of monovalent cation sizes; the ratio of the size of the sphere is proportional to cation size. (D) M^+/Zn^{2+} ratio in the electrode after five charge–discharge cycles. The ratios were determined by digesting the electrode after five charge–discharge cycles, following washing with THF, and quantifying the corresponding metal content by ICP-OES (Tables S1 and S2).

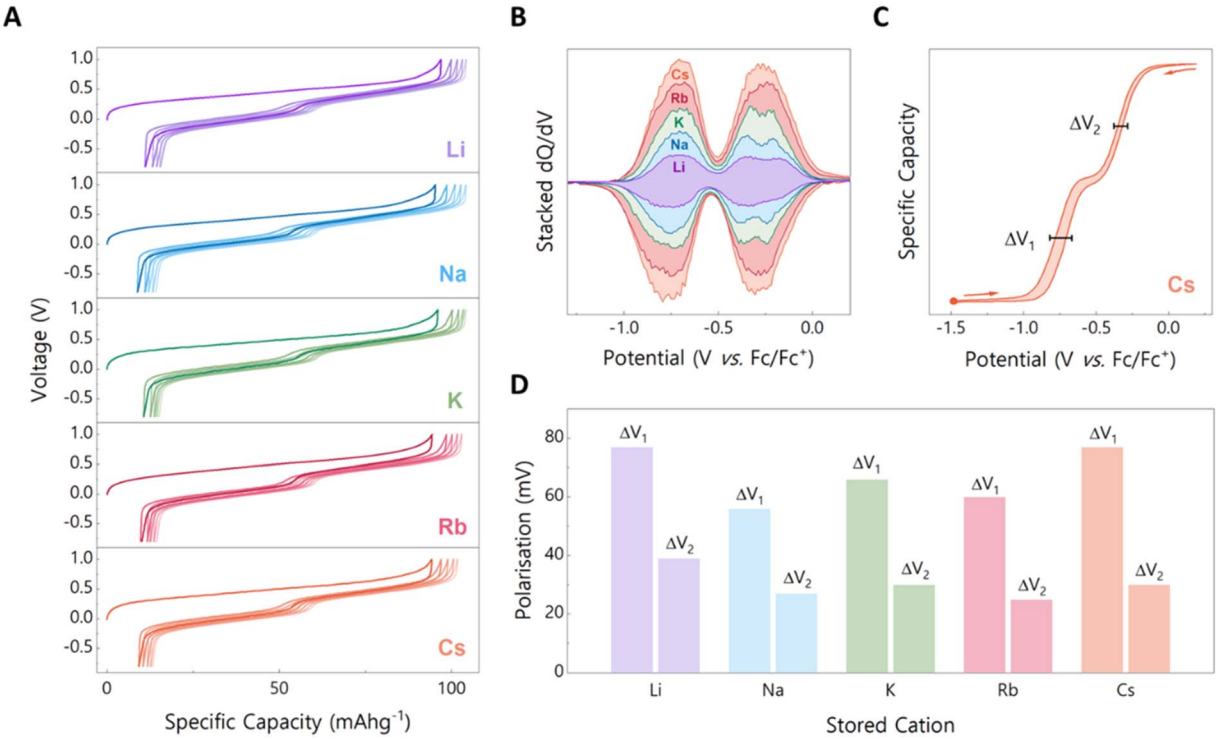

Fig. 2 (A) Galvanostatic charge–discharge profiles over the first five cycles using Ca–Zn–PTtSA as positive electrode material for Li^+, Na^+, K^+, Rb^+, and Cs^+ storage. Electrolyte used was 1 mol L^{-1} MTFSI in propylene carbonate electrolyte; electrodes cycled at current density of 10 mA g^{-1} in a three-electrode Ca–Zn–PTtSA||Ag||AC cell. (B) The corresponding dQ/dV plots at cycle 5, stacked on top of each other with a rescaling factor of 2 for visibility. (C) Charge–discharge polarization estimation for Cs^+ storage, as determined at the cycle 5, for a current density of 10 mA g^{-1}; a larger hysteresis is noted for the 1st redox plateau. (D) Comparative analysis of polarization values of the 1st and 2nd plateaus for each 1s-block cation system studied; as determined at the cycle 5, for a current density of 10 mA g^{-1}.

Rb^+ and Cs^+) is preferentially stored during the subsequent cycling, yielding the corresponding M_2–Zn–PTtSA phases. To ensure complete substitution of Ca^{2+} by M^+, the electrode is cycled at low active material loading (1.5 mg) in a large excess of electrolyte (250 μL). Under these testing conditions, the M^+/Ca^{2+} ratio in the electrolyte is ∼100, which drives the full cation exchange in the electrode matrix (Fig. 1B). This preferential storage of M^+ over Ca^{2+} is further driven by the slightly higher mobility of M^+, owing to its lower charge density.[23,24] The full substitution of Ca^{2+} was confirmed by elemental analysis of the electrodes after 5 charge–discharge cycles, which showed an M^+/Zn^{2+} ratio of ∼1.95 (Fig. 1D), with Ca^{2+} remaining only at trace levels (Tables S1, and 2). To validate this result, a control experiment was carried out by electrochemically extracting Ca^{2+}, removing and washing the electrode, and then assembling a fresh cell with M^+ electrolyte. The electrochemical performances obtained in this configuration were identical to that observed for *in situ* replacement of Ca^{2+} by M^+ (Fig. S1).

Electrochemical analysis of M^+ storage

A systematic study of all M^+ systems requires a universal counter electrode that is not influenced by the nature of the stored ions. For this purpose, a capacitive carbon counter electrode was employed. Since the charge storage is capacitive, it is minorly affected by the specific cation adsorbed at the surface.[25] Capacitive carbon is commonly used as a counter electrode in divalent systems, where the corresponding metal anodes are unsuitable due to passivation layer formation. This approach eliminates artifacts that could otherwise arise from using metal anodes as counter electrodes.[25] The galvanostatic cycling analyses of Ca–Zn–PTtSA in corresponding M^+ electrolytes revealed a specific capacity of ∼95 mAh g^{-1} for all alkali cations, corresponding to full material utilization (Fig. 2A). This observation is consistent with elemental analysis of cycled electrodes (Fig. 1D), which confirmed complete exchange of Ca^{2+} by M^+. This makes Ca–Zn–PTtSA a rare example of positive electrode material capable of efficiently storing large cations, such as Rb^+ and Cs^+.

Achieving such full utilization across the entire cation series is remarkable, as larger cation sizes are usually considered to reduce accessibility and slower diffusion, resulting in a drop in material utilization. For example, in polyanthraquinones, the material utilization decreases by nearly 50% when moving from Li^+ to Ca^{2+} storage, while in olivine iron phosphate phases ($FePO_4$) it drops by ∼25% between Li^+ and K^+.[12,19] Layered ruthenium- and cobalt-based oxides have also been investigated as positive electrode materials for large cations such as Cs^+ and Rb^+. Although these can accommodate such ions, their practical utilization remains very limited, below 20% of the theoretical capacity, due to the large ionic size of the cations, which restricts their intercalation into the layered structures.[28] In

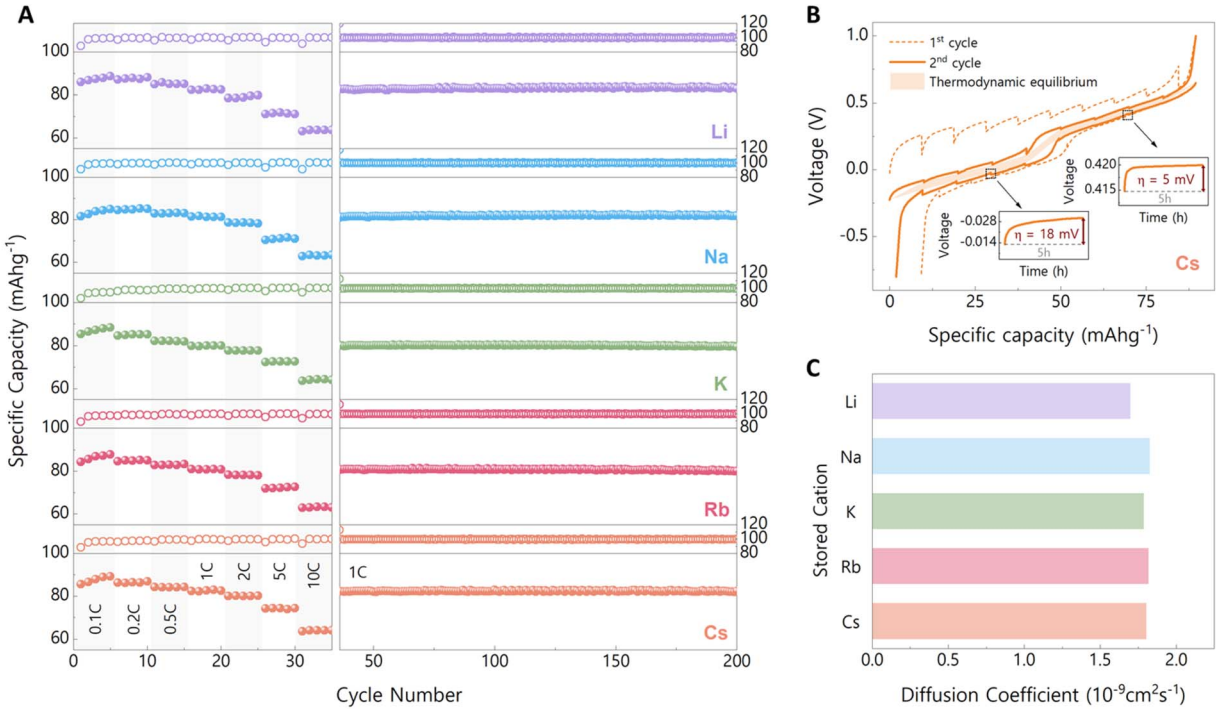

Fig. 3 (A) C-rate performance and long-term cycling stability of M_2–Zn–PTtSA electrode materials. (B) GITT plot of Ca–Zn–PTtSA pristine electrode materials during the first two cycles (and cation exchange) operated at a current density of 10 mA g^{-1} for Cs^+ storage, with a 5 h relaxation period following every 1 h duration of current injection or extraction. The insets show the OCV evolution during relaxation periods within the high-potential and low-potential plateau regimes. (C) Average diffusion coefficients for M_2–Zn–PTtSA materials, as determined from GITT analysis.

contrast, M_2–Zn–PTtSA shows no size-dependent limitations: the material utilization remaining essentially unaffected by the nature of the stored cation.

This observation is further supported by the galvanostatic charge–discharge profiles, which are highly similar for all M^+ ions (Fig. 2A). The difference observed between the first and subsequent cycles is not related to Ca^{2+}/M^+ exchange but is intrinsic to the material itself. Specifically, during synthesis, Ca^{2+} is coordinated in a particular configuration within the polymer. Upon electrochemical cycling, reinsertion occurs in a different configuration, which enhances Ca^{2+} mobility and reduces the overpotential, as previously reported.[7,15] Beyond the first charge activation step, all systems exhibit two sloping plateaus in the voltage profiles, corresponding to the sequential reversible two-electron redox process of the $PTtSA^{4-}$ ligand.[7,8] To evaluate and compare the working voltages of the different M^+ systems, differential capacity (dQ/dV) plots were extracted from the galvanostatic cycling experiments, measured in a 3-electrode cell with a silver wire as pseudo-reference electrode (Fig. 2B). All M^+ cations exhibit very similar dQ/dV profiles, with two well-defined redox peaks corresponding to the sequential two-electron redox processes of the $PTtSA^{4-}$ ligand. Remarkably, no peak shift is observed across the different M^+ systems, indicating that the redox potential remains essentially identical for all stored cations, at about −0.55 V *vs.* Fc/Fc^+ (Fig. S2). This corresponds to ~3.1 V *vs.* Li^+/Li or ~2.8 V *vs.* Na^+/Na, which was independently verified by assembling a Li-metal and Na-metal half-cell that yielded same average discharge potentials (Fig. S3, and S4). Such invariance of the redox potential is consistent with the nature of the coordination polymer: the electronic charge being strongly delocalized, the counter cations (M^+) remain weakly bound, with limited impact on the electron density of the ligand.

Another parameter typically influenced by the nature of the stored cation is the voltage hysteresis between charge and discharge steps. In most systems, hysteresis increases with cation size, as larger ions diffuse more slowly and face higher kinetic barriers.[21,24,26] For instance, in PTtSA-based systems, the hysteresis between Li_4–PTtSA and K_4–PTtSA differs by ~100 mV, while in $FePO_4$ the use of K^+ instead of Li^+ increases hysteresis by nearly 300 mV.[12] In sharp contrast, M_2–Zn–PTtSA exhibits low hysteresis for all M^+ cations, comparable to what has been reported for Ca^{2+} storage (Fig. 2C and D).[15] Specifically, the hysteresis is ~70 mV for the first plateau and ~30 mV for the second, when material is used at a current density of 10 mA g^{-1}. This behavior is explained by two structural features of Ca–Zn–PTtSA: (i) an amorphous open framework, which provides flexibility to accommodate large cations, and (ii) the weak interaction between the cations and the host structure, enabled by electron delocalization within the organic linker.

These key features of conjugated sulfonamide coordination polymer also account for their excellent rate capability and long-term cycling stability (Fig. 3A). The combination of weak cation–host interactions and a flexible amorphous backbone facilitate

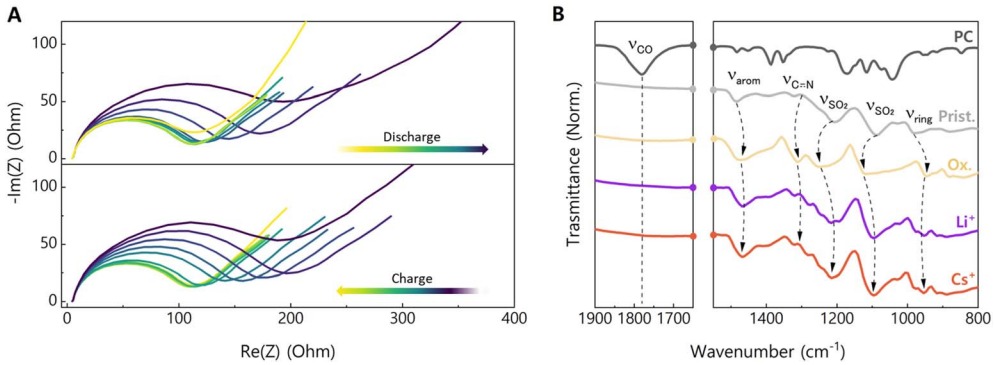

Fig. 4 (A) *In situ* electrochemical impedance spectroscopy (EIS) collected during the second charge and discharge cycle of the Ca–Zn–PTtSA electrode using 1 mol L^{-1} KTFSI in propylene carbonate as electrolyte, and at a current density of 10 mA g^{-1}. One EIS spectrum was recorded after each electrochemical step, consisting of 1 h of charge or discharge followed by a 1 h rest period. (B) *Ex situ* FTIR spectra of the pristine Ca–Zn–PTtSA (Prist.), electrochemically oxidized □-Zn–PTtSA (Ox.), electrochemically reduced Li_2–Zn–PTtSA (Li^+), and Cs_2–Zn–PTtSA (Cs^+) phases, overlayed with the propylene carbonate spectra to highlight characteristic bands.

rapid M^+ diffusion, enabling efficient charge storage even at high current densities. As a result, the material retains ~60% of its capacity at a rate of 10C. Galvanostatic intermittent titration technique (GITT) measurements further confirm the fast ion transport, yielding diffusion coefficients on the order of 2×10^{-9} cm^2 s^{-1} (Fig. 3B, C, S5 and S6). To note that these values exceed those typically reported for Li^+ diffusion in benchmark inorganic electrodes such as LFP and layered NMC oxides, highlighting the peculiar transport properties of the amorphous sulfonamide framework.[27] Interestingly, the diffusion coefficients remain similar across the series of cations from Li^+ to Cs^+. This apparent invariance likely results from a balance of two opposing effects: as the cation size increases, diffusion should slow down due to steric constraints, yet the lower charge density of larger cations reduces the interaction with the polymer backbone, facilitating transport. These competing factors effectively counteract one another, yielding comparable diffusion coefficients for all M^+ cations. This finding aligns with the C-rate tests, as any difference in ion diffusion between cations would have led to corresponding variations in capacity retention.

In terms of long-term cycling, all M^+ systems demonstrate good stability at a 1C rate, with capacity retention exceeding 99.9% and coulombic efficiencies consistently above 99.9%. Such stability is unusual for large cation storage, which typically lead to rapid capacity fading. In many electrode materials, once the large cation is extracted, the framework undergoes partial collapse or irreversible structural rearrangements, making subsequent reinsertion increasingly difficult.[26] For instance, in $FePO_4$, Li^+ storage delivers excellent stability with >99% capacity retention over 50 cycles, but when K^+ is stored, retention drops drastically to ~80% over the same duration.[12] By contrast, the amorphous and flexible framework of Ca–Zn–PTtSA tolerates the insertion and removal of large cations without undergoing such collapse, thereby maintaining both structural integrity and electrochemical reversibility. This intrinsic resilience explains the nearly perfect capacity retention observed across the full series of 1s block cations, from Li^+ to Cs^+.

To further investigate the charge-storage mechanisms associated with the different M^+ cations, *in situ* electrochemical impedance spectroscopy (EIS) was performed for each system (Fig. 4A and S7). The K^+ storage is discussed here as a representative example, as similar trends were observed for all investigated cations. As shown in Fig. 4A, during charge the overall cell resistance progressively decreases, reaching a minimum at the end of charge. Assuming that the contributions from electrochemically inactive cell components remain relatively constant during cycling (separator, electrolyte, current collectors), this decrease in resistance can be attributed to changes occurring at the positive electrode. The observed decrease in resistance is consistent with an increase in the electronic conductivity of the electrode material upon progressive oxidation. In principle, oxidation and extraction of K^+ ions from the positive electrode framework are expected to reduce the ionic conductivity, which should lead to an increase in cell resistance. However, in the present case, the enhancement of electronic conductivity clearly outweighs the decrease in ionic conductivity, resulting in an overall reduction in the measured resistance. This behavior can be rationalized by considering the structural and electronic modifications induced by oxidation. The removal of cations from the framework enables a more favorable alignment between the PTtSA ligands and the Zn^{2+} centers. Moreover, oxidation of the ligand promotes electronic delocalization, improving orbital overlap, and thereby enhancing charge–transport properties within the coordination polymer.[6] Upon discharge, the resistance progressively increases and returns to the initial value measured at the beginning of the charge. This trend is consistent with the reduction of the material and the associated decrease in electronic conductivity as the system returns to its reduced state. The same qualitative mechanism is observed for all cation-storage systems investigated in this study. However, a direct and quantitative comparison between different stored cations remains challenging. The measured impedance reflects the combined contributions of all cell components, particularly the

electrolyte, and the interfaces, which differ between systems and can influence the overall cell resistance.

Complimentary, *ex situ* FTIR analysis was performed on electrochemically cycled electrodes to investigate the redox and ion-storage mechanisms (Fig. 4B and S8). During oxidation, the sulfonamide bands shift toward higher wavenumbers, corresponding to the extraction of calcium ions from the coordination polymer and the resulting increase in electron density on the S=O groups (1207 and 1085 cm^{-1}). A new vibrational band associated with the C=N bond appears upon oxidation (1312 cm^{-1}), consistent with the Wurster-type redox process of the $PTtSA^{4-}$ ligand.[6] Upon discharge, the C=N vibrational band disappears, and the sulfonamide bands shift back toward lower wavenumbers, indicating the recoordination of metal ions to the sulfonamide groups. Interestingly, the sulfonamide bands observed for Li^+ and Cs^+ storage are identical (1095 cm^{-1}) but slightly shifted compared to the pristine material (1085 cm^{-1}); with similar trend observed across the full M_2–Zn–PTtSA series (Fig. S8). This shift can be attributed to the difference in charge between monovalent and divalent cations, with the latter exhibiting a stronger polarizing power character. These spectroscopic results align with the electrochemical performance, as no major differences were observed among the various cations, suggesting weak and reversible metal–ligand coordination in all cases. Moreover, no propylene carbonate bands were detected in any discharged electrodes (Fig. 4 and S8).[28,29] Together with elemental analysis confirming the absence of anion co-intercalation (Fig. 1), these results demonstrate that Li^+, Na^+, K^+, Rb^+, and Cs^+ are stored in pure solid-state (non-solvated) within the coordination polymer framework.

The electrochemical cation-exchange approach developed here was primarily used to investigate the impact of the stored cation on the electrochemical performance, while avoiding artefacts that may arise from material synthesis. Indeed, synthesis can lead to variations in phase purity, polymer chain length, and related structural features, which can have an impact performance. However, this approach is not ideally suited for practical cell design. To address this limitation, equivalent coordination polymers, analogous to Ca–Zn–PTtSA but incorporating the cation of interest, can instead be obtained directly through chemical synthesis. As representative examples, we explored here the direct chemical synthesis of Na_2–Zn–PTtSA and Cs_2–Zn–PTtSA. These can be obtained through an acid–base reaction followed by cation exchange, similarly to the reported synthesis of Ca–Zn–PTtSA (the detailed synthesis is described in the SI). The electrochemical performance of these chemically synthesized derivatives was found to be equivalent to that obtained through electrochemical cation exchange (Fig. S9).

Conclusions

In summary, the amorphous Ca–Zn–PTtSA coordination polymer serves as a universal host for reversible electrochemical accommodation of all alkali-metal cations from Li^+ to Cs^+, including the rare case of reversible Rb^+ and Cs^+ storage. Across the series, the materials achieve full utilization with similar redox potentials and low polarization, highlighting an unusual level of cation versatility among organic and inorganic electrodes. Independent of cation size, storage proceeds *via* a purely solid-state mechanism without solvent co-intercalation. The combination of an amorphous, flexible framework and a delocalized electronic structure support weak and reversible metal–ligand interactions, enabling fast ion transport and stable cycling even for large cations. Finally, direct chemical synthesis of Na_2–Zn–PTtSA and Cs_2–Zn–PTtSA yields electrochemical behavior comparable to that obtained *via* electrochemical cation exchange, supporting future development of practical post-lithium battery systems.

Author contributions

All authors contributed to the conception of the study, data analysis and interpretation, and manuscript preparation, and all authors have approved the final version of the manuscript.

Conflicts of interest

The authors declare no competing interests.

Data availability

No software or code was generated in this study. All data supporting the findings of this work are provided in the supplementary information (SI). The data that support the findings of this study are also available from the corresponding author upon reasonable request. Supplementary information: experimental procedures and characterization; cell assembly and electrochemical testing protocols; additional figures and tables. See DOI: https://doi.org/10.1039/d6sc00585c.

Acknowledgements

This work was supported by F. R. S.-FNRS under the Excellence of Science program (EOS 40007515); WEL Research Institute (grant X.9008.25 – HECTOR); PDR research project (T.0418.26 ORANGE); European Research Council under the European Union's Horizon 2020 research and innovation program (grant agreement No. 770870, MOOiRE); and R.8001.24 COBRA grant, a M-ERA.NET 3 funding from EU Horizon 2020, GA No. 958174. D. R. acknowledgeiks F. R. S.-FNRS for Chargé de Recherché (CR) fellowship (grant agreement No. 1.B.098.23). R. M. acknowledges FRS-FNRS for PhD fellowships (grant agreement No. 1.A.836.23).

References

1 A. E. Lakraychi and A. Vlad, Organic, Batteries-the route towards sustainable electrical energy storage technologies, *Chem. Nouv.*, 2018, **127**, 1–9.
2 Y. Lu and J. Chen, Prospects of organic electrode materials for practical lithium batteries, *Nat. Res.*, 2020, **4**, 127–142.

3 H. Kim, J. E. Kwon, B. Lee, J. Hong, M. Lee, S. Y. Park and K. Kang, High Energy Organic Cathode for Sodium Rechargeable Batteries, *Chem. Mater.*, 2015, **27**, 7258–7264.
4 Y. Xu, M. Zhou and Y. Lei, Organic materials for rechargeable sodium-ion batteries, *Mater. Today*, 2018, **21**, 60–78.
5 A. E. Lakraychi, F. Dolhem, A. Vlad and M. Becuwe, Organic Negative Electrode Materials for Metal-Ion and Molecular-Ion Batteries: Progress and Challenges from a Molecular Engineering Perspective, *Adv. Energy Mater.*, 2021, **11**, 2101562.
6 J. Wang, A. E. Lakraychi, X. Liu, L. Sieuw, C. Morari, P. Poizot and A. Vlad, Conjugated sulfonamides as a class of organic lithium-ion positive electrodes, *Nat. Mater.*, 2021, **20**, 665–673.
7 J. Wang, X. Guo, P. Apostol, X. Liu, K. Robeyns, L. Gence, C. Morari, J. F. Gohy and A. Vlad, High performance Li-, Na-, and K-ion storage in electrically conducting coordination polymers, *Energy Environ. Sci.*, 2022, **15**, 3923–3932.
8 J. Wang, X. Liu, H. Jia, P. Apostol, X. Guo, F. Lucaccioni, X. Zhang, Q. Zhu, C. Morari, J. F. Gohy and A. Vlad, High performance Li-, Na-, and K-ion storage in electrically conducting coordination polymers, *ACS Energy Lett.*, 2022, **7**, 668–674.
9 R. Verrelli, A. Black, R. Dugas, D. Tchitchekova, A. Ponrouch and M. R. Palacin, Steps Towards the Use of TiS_2 Electrodes in Ca Batteries, *J. Electrochem. Soc.*, 2020, **167**, 070532.
10 A. Ponrouch, J. Bitenc, R. Dominko, N. Lindahl, P. Johansson and M. R. Palacin, Multivalent rechargeable batteries, *Energy Storage Mater.*, 2019, **20**, 253–262.
11 L. Han, K. Chen, X. Chen, Y. Zhao, M. Li, C. Liu, Y. Cao and Y. Fang, A 3.7 V amorphous $Na_2VO(SO_4)_2$ cathode with boosted electrode kinetics for advanced sodium-ion batteries, *Nano Energy*, 2025, **139**, 110986.
12 V. Mathew, S. Kim, J. Kang, J. Gim, J. Song, J. P. Baboo, W. Park, D. Ahn, J. Han, L. Gu, Y. Wang, Y. S. Hu, Y. K. Sun and J. Kim, Amorphous iron phosphate: potential host for various charge carrier ions, *NPG Asia Mater.*, 2014, **6**, 138.
13 J. Bitenc, K. Pirnat, O. Lužanin and R. Dominko, Organic Cathodes, a Path toward Future Sustainable Batteries: Mirage or Realistic Future?, *Chem. Mater.*, 2024, **36**, 1025–1040.
14 Y. Zhang, J. Wang, P. Apostol, D. Rambabu, A. Eddine Lakraychi, X. Guo, X. Zhang, X. Lin, S. Pal, V. Rao Bakuru, X. Chen and A. Vlad, Bimetallic Anionic Organic Frameworks with Solid-State Cation Conduction for Charge Storage Applications, *Angew. Chem.*, 2023, **62**, 202310033.
15 X. Guo, R. Markowski, A. Black, P. Apostol, D. Rambabu, O. Lužanin, T. Pavčnik, D. Monti, M. Du, D. Tie, X. Lin, V. R. Bakuru, R. Delogne, K. Robeyns, L. Simonelli, J.-F. Gohy, J. Bitenc, J. Wang, A. Ponrouch and A. Vlad, Amorphous coordination polymers for versatile Mg^{2+}, Ca^{2+}, Sr^{2+}, Ba^{2+}, and Zn^{2+} cation storage, *Energy Environ. Sci.*, 2025, **18**, 9114–9124.
16 T. Kawaguchi, H. Sakurai, S. Fukui, X. Ye, H. Li, T. Mandai, N. L. Okamoto and T. Ichitsubo, Amorphous oxide cathode enabling room-temperature rechargeable magnesium batteries, *Commun. Mater.*, 2025, **6**, 203.
17 J. Ding, D. Ji, Y. Yue and M. M. Smedskjaer, Amorphous Materials for Lithium-Ion and Post-Lithium-Ion Batteries, *Small*, 2024, **20**, 2304270.
18 B. Pan, J. Huang, Z. Feng, L. Zeng, M. He, L. Zhang, J. T. Vaughey, M. J. Bedzyk, P. Fenter, Z. Zhang, A. K. Burrell and C. Liao, Polyanthraquinone-Based Organic Cathode for High-Performance Rechargeable Magnesium-Ion Batteries, *Adv. Energy Mater.*, 2016, **6**, 1600140.
19 O. Lužanin, A. K. Lautar, T. Pavčnik and J. Bitenc, Paving the way for future Ca metal batteries through comprehensive electrochemical testing of organic polymer cathodes, *Mater. Adv.*, 2023, **5**, 642–651.
20 B. Flamme, B. Jismy, M. Abarbri and M. Anouti, Poly-anthraquinone sulfide isomers as electrode materials for extended operating temperature organic batteries, *Mater. Adv.*, 2021, **2**, 376383.
21 D. Monti, N. Patil, A. P. Black, D. Raptis, A. Mavrandonakis, G. E. Froudakis, I. Yousef, N. Goujon, D. Mecerreyes, R. Marcilla and A. Ponrouch, Polyimides as Promising Cathodes for Metal–Organic Batteries: A Comparison between Divalent (Ca^{2+}, Mg^{2+}) and Monovalent (Li^+, Na^+) Cations, *ACS Appl. Energy Mater.*, 2023, **6**, 7250–7257.
22 V. R. Bakuru, P. Apostol, D. Rambabu, S. Pal, X. Lin, R. Markowski, T. Goossens, D. Tie, A. Kachmar, Y. Zhang, G. Chanteux and A. Vlad, A hexaanionic carboxyphenolate framework for high energy alkali cation storage, *Energy Environ. Sci.*, 2025, **18**, 6131–6140.
23 J. D. Forero-Saboya, E. Marchante, R. B. Araujo, D. Monti, P. Johansson and A. Ponrouch, Cation Solvation and Physicochemical Properties of Ca Battery Electrolytes, *J. Phys. Chem. C*, 2019, **123**, 29524–29532.
24 A. Ponrouch and M. Rosa Palacín, Post-Li batteries: promises and challenges, *Philos. Trans. R. Soc., A*, 2019, **377**, 20180297.
25 R. Dugas, J. D. Forero-Saboya and A. Ponrouch, Methods and Protocols for Reliable Electrochemical Testing in Post-Li Batteries (Na, K, Mg, and Ca), *Chem. Mater.*, 2019, **31**, 8613–8628.
26 D. S. Tchitchekova, C. Frontera, A. Ponrouch, C. Krich, F. Bardé and M. R. Palacín, Electrochemical calcium extraction from 1D-$Ca_3Co_2O_6$, *Dalton Trans.*, 2018, **47**, 11298–11302.
27 M. Park, X. Zhang, M. Chung, G. B. Less and A. M. Sastry, A review of conduction phenomena in Li-ion batteries, *J. Power Sources*, 2010, **195**, 7904–7929.
28 G. A. Ferrero, G. Åvall, K. Janßen, Y. Son, Y. Kravets, Y. Sun and P. Adelhelm, Solvent Co-Intercalation Reactions for Batteries and Beyond, *Chem. Rev.*, 2025, **125**, 3401–3439.
29 Y. Ein Ely, D. Aurbach, M. Babai and Y. Carmeli, Electrochemical and spectroscopic studies of carbon electrodes in lithium battery electrolyte systems, *J. Power Sources*, 1993, **43**, 47–63.